Origin of the Photoinduced Optical Second Harmonic Generation Arising in *N*-Phenyl Microcrystalline Films

M. Makowska-Janusik, S. Tkaczyk, and I. V. Kityk*

Institute of Physics, J. Dlugosz University, Al.Armii Krajowej 13/15, 42-200 Czestochowa, Poland

Received: October 21, 2005; In Final Form: January 19, 2006

Photoinduced second-order nonlinear optical effects, particularly optical second harmonic generation (SHG) of *N*-phenyls with different numbers of aromatic rings deposited on glass substrates were studied. As a fundamental beam, a 5-ps pulsed Nd:YAG laser was used. Quantum chemical time-dependent density functional theory (TDDFT) simulations of the nonlinear optical properties were performed. The first-order hyperpolarizabilities of isolated molecules were calculated, under the influence of a polarized pumping beam, to evaluate the role played by the nanointerfaces separating the microcrystallites and the amorphous environment. Consideration was performed within a framework of steady-state Langevin order parameters for amorphous-like films. A strong dependence of the photoinduced SHG versus the number of aromatic rings determining the degree of film crystallinity was shown. A comparison of experimental data and theoretically evaluated results shows that for the photoinduced first-order nonlinear optical effect the dominant contribution is an amorphous-like structural component, unlike the transport properties, where the crucial role is played by the nanointerface region. This may reflect a specific feature of the multiphoton processes in such types of nanointerfaces because of nanoconfined effects.

Introduction

Recently, π-conjugated organic and polymeric systems have been studied intensively because of their promising applications in optoelectronic and quantum optical devices and different kinds of optical switchers.[1,2] Structures simultaneously possessing long-range ordered fragments (microcrystallites), an amorphous-like (disordered) background and, as a consequence, interface regions between them, usually with nanoscale sizes, present particular interest. The coexistence of structures possessing different homogeneities within one sample should play a crucial role in its optical and electronic properties. Interaction of the external electric (polarized optical) field with the medium gives different time- and space-dependent dielectric permittivity depending on the amount of particular structural fragments and their electronic properties. Hence, *N*-phenyl microcrystalline films deposited on glass substrates seem to be promising materials for experimental as well as for fundamental theoretical investigations.[3,4] They possess the coexistence of microcrystalline areas with different degrees of film crystallinity depending on the number of aromatic rings, an amorphous-like background, and the nanointerface region for the same sample. Typical AFM pictures of the two studied film *N*-phenyl samples are presented in Figure 1. As a consequence of structural nonhomogeneity, one can expect substantially different photoinduced optical responses from different parts of the films. It is clear that in this case a coexistence of delocalized quasi-band energy states and highly localized nanoconfined states exist. In previous works[5,6] we have established that the thin nanointerface layers (about several nanometers) separating the crystallites and amorphous-like background give a predominant contribution to the observed DC electric transport properties; hence, they cover only a several volume percent compared with the total volume of the composites. Varying the film thickness was an opportunity to vary the microcrystalline sizes as well as the interface thickness. It is also important that the thin nanoconfined states may be crucial for manifestation of the interesting optical and nonlinear optical properties.[7]

Using TDDFT simulations together with a method of molecular dynamics simulations taking into account polarized photoinduced light we have investigated the considered *N*-phenyls to establish the role of their main structural fragments in the nonlinear optical response. Generally, the SHG phenomena described by third rank polar tensor, for disordered media, are forbidden by symmetry. So, to obtain noncentrosymmetry charge density distribution together with appropriate phase-matching conditions it is necessary to create long-range alignment of the molecular dipole moments (both state as well transition ones). It can be achieved by applying an external electric field (electric-field induced SHG) or using the polarized induced optical field (photoinduced SHG). However, because of the coexistence of the crystalline structure and nanointerfaces, the SHG effect may substantially depend on the sizes of the nanoconfined states, which may contribute efficiently to nonlinear optical susceptibility response. During photoalignment it is necessary to investigate order parameters as a consequence of the deviation of the molecular dipole moment direction from the direction of the photoinducing polarized electromagnetic wave.

The dipole orientation order parameters determining the SHG for one-dimensional molecules are $\langle \cos \theta \rangle$ and $\langle \cos^3 \theta \rangle$, where θ is the angle between the molecular dipole moment and the external effective polarizing electric field, determined by polarization of induced optical pump beam. The order parameters can be evaluated by a method of molecular dynamics and may be compared with the theoretically predicted odd-order Langevin functions, $L_1(p)$ and $L_3(p)$.[8]

In the present work we perform experimental measurements of the first-order NLO properties, particularly photoinduced SHG, for different *N*-phenyl samples and carry out their

10.1021/jp056029c CCC: $33.50
Published on Web 03/11/2006

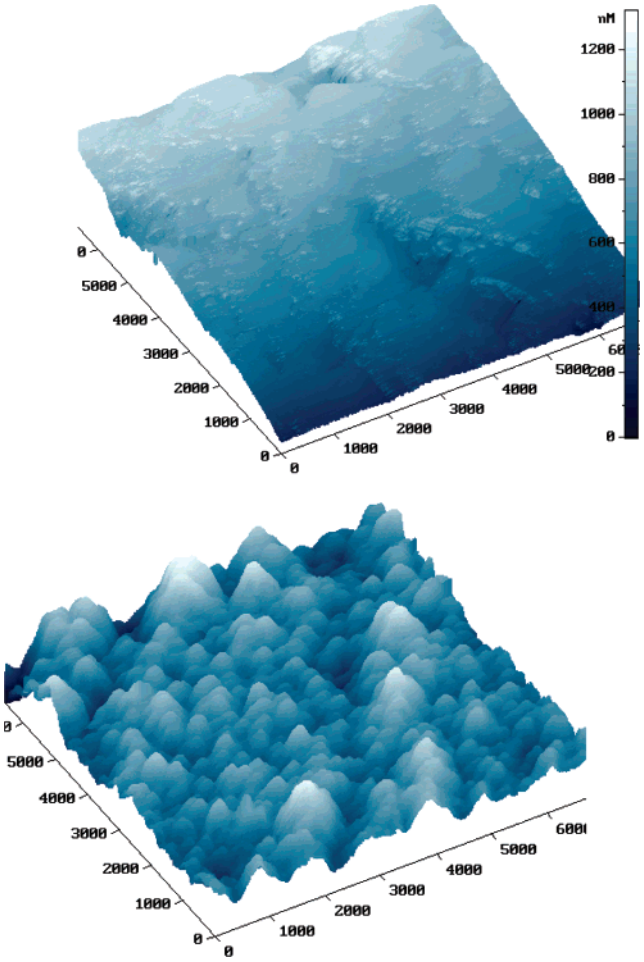

Figure 1. Typical AFM pictures for two investigated materials; *p*-therphenyl at the top and *p*-sexiphenyl at the bottom.

theoretical investigations. TDDFT quantum chemical calculations together with appropriate molecular dynamics simulations substantially improve our understanding of the physical insight of the electronic process. Using theoretically evaluated odd-order Langevin functions $L_1(p)$ and $L_3(p)$, we predict the electric field behavior of the first-order hyperpolarizability. Experimentally, we explore the key representatives of the *N*-phenyls: ter- ($N = 3$), quarter- ($N = 4$), quinque- ($N = 5$), and sexiphenyl ($N = 6$) possessing different degrees of long-range ordering. The additional molecule-like biphenyl ($N = 2$) was studied only theoretically.

The main goal of this paper consists of quantum chemical simulation of the photoinduced SHG in *N*-phenyl films and comparison with the experimental results. Comparison of experimental SHG data with theoretically simulated data are a criterion of the applicability of the theoretical simulations and should play a principal role in the clarification of the basic mechanisms. First of all, the geometry optimization of the considered molecules has been performed. The principal goal of the present work consists of clarification of the contribution of particular structural fragments (amorphous-like phase, crystalline and nanointerfaces) of the films to the observed nonlinear optical effects in *N*-phenyl films.

Theoretical Simulations

Details of Quantum Chemical Calculations. All of the simulated electronic properties of the investigated molecules were calculated within a framework of TDDFT utilizing the Amsterdam Density Functional (ADF) [10] program package. The DFT approach gives good results for the simulation of electronic properties for many-electron systems; however, for evaluations of optical polarizability as well as hyperpolarizability $\beta(-2\omega;\omega,\omega)$, the TDDFT[10,11] approach is appropriate, which is presented in the ADF-RESPONSE module.[12] Generally, the TDDFT is more appropriate than oversimplified two- and three-level models because the complication of the exciting level calculations and over-the-state summation is replaced by a more theoretically strong procedure using the perturbation theory of the local charge density. The principal advantages of the TDDFT compared to the traditional DFT approach consists of a successive overcoming of complications related to the repulsion of energetically close electronic excited levels. It is also necessary to emphasize that the TDDFT calculations reproduce the experimental hyperpolarizability spectra well for small molecules.[13] The only known case in which the NLO TDDFT calculations are currently unsatisfactory occurs for long linear chains, and current DFT should be applied (shown in ref 14).

The exchange-correlation (xc) functional potential was chosen in a form of gradient-regulated asymptotic correction (GRAC) potential[15] presenting a gradient-regulated relation between the generalized gradient approximation (GGA) introduced by Becke and Perdew (BP86) and the asymptotically corrected Leeuwen−Baerends potential (LB94). Additional calculations using the basic local density approximation (LDA), corresponding to the local Slater exchange function, together with uniform local gas correlation functional of Vasko, Wilk, and Nusair,[16] yielded values similar to those obtained with the GRAC potential. The ionization potentials (necessary for GRAC calculations) were computed from the difference between the energies of the neutral and singly ionized cations, evaluated at the BLYP level, and were found to be equal to 7.06, 6.49, 6.14, 5.90, and 5.71 eV for biphenyl, terphenyl, quaterphenyl, quinquephenyl, and sexiphenyl, respectively. The adiabatic local density approximation (ALDA) was used for the xc Kernel, which describes the first-order response of the xc potential under applied external electric field. The ADF uses a Slater-type orbital (STOs) basis set, and in the present work an all-electron doubly polarized valence triple-ζ basis set (TZ2P) has been chosen.[17] All of the molecules were rotated to align the maximal state ground dipole moment along the *z* axis. Before calculations of the electronic properties were performed, we optimized the molecular stereochemistry of the isolated molecules at the restricted Hartree−Fock (RHF) level using the ADF package. The GGA part of the xc functional potential was calculated with the Perdew correlation term[18] and the Becke gradient correction[19] for the exchange part of potential assuming C_1 symmetry.

Simulations of SHG Intensity versus the Orientation of the *N*-Phenyl Molecules Relation. All of the molecules used in the present work are rodlike in shape. The first-order nonlinear optical susceptibility depends on the random reorientation of active molecules. It can be related to the molecular hyperpolarizability by

$$\chi_{ZZZ}(-2\omega;\omega,\omega) = \frac{NL(2\omega)\,L^2(\omega)}{4\epsilon_0} \left[2\beta_{zzz}(-2\omega;\omega,\omega)\langle\cos^3\theta\rangle + \sum_{i=x,y} (\beta_{zii}(-2\omega;\omega,\omega) + 2\beta_{iiz}(-2\omega;\omega,\omega))\langle\cos\theta - \cos^3\theta\rangle \right] \quad (1)$$

$$\chi_{Z\perp\perp}(-2\omega;\omega,\omega) = \frac{NL(2\omega)\,L^2(\omega)}{8\epsilon_0}\begin{bmatrix} 2\beta_{zzz}(-2\omega;\omega,\omega)\langle\cos\theta - \cos^3\theta\rangle \\ +\sum_{i=x,y}\beta_{zii}(-2\omega;\omega,\omega)\langle\cos\theta + \cos^3\theta\rangle \\ -\sum_{i=x,y}2\beta_{iiz}(-2\omega;\omega,\omega)\langle\cos\theta - \cos^3\theta\rangle \end{bmatrix} \quad (2)$$

where $L(\omega)$ and $L(2\omega)$ are local field factors, the $\langle\ \rangle$ brackets represent the average over space orientation distribution of the molecules, and β_{ijk} is the first-order nonlinear hyperpolarizability. The thermal disordering requires the assumption that the reorientation of the molecules has the Boltzman-like distribution.[20] The order parameters $\langle\ \rangle$ computed over the Boltzman distribution correspond to the odd-order Langevin functions.[8]

Experimental Measurements

Preparation of the Samples. The *N*-phenyl films for all of the considered samples were obtained by a vacuum sublimation (at pressure about 6.5×10^{-6} Torr) on a BK7 glass used as a substrate. The thickness of the evaporated films was varied from 0.2 up to 2.5 μm and their space nonhomogeneity (due to distribution of the microcrystallites) controlled by UV-absorption spectrophotometery did not exceed 0.2%. As row materials for film deposition of all of the considered samples the powders with chemical purity of 99% *m*-terphenyl (1,3-diphenylobenzene) produced by Tokyo Kasei Co. Ltd. Japan, were used: namely, $C_{36}H_{26}$ (with molecular mass 458.59 amu), $C_{30}H_{22}$ (382.50 amu), $C_{24}H_{18}$ (306.41 amu), and $C_{18}H_{14}$ (230.31 amu).

It was found that during the vacuum sublimation the radial-oriented appeared microcrystallized morphology with slightly agglomerated spheroids.[7] The microcrystalline X-ray diffractograms of all of the considered samples are given in Figure 2. One can see substantially different crystallinity of the ter- and quarterphenyl films compared to the more disordered quinque- and sexiphenyl.

Photoinduced Second Harmonic Generation Technique. A principal setup for the photoinduced SHG measurements is presented in Figure 3. As a fundamental beam, we used a 5-ps pulsed Nd:YAG laser ($\lambda = 1.06\ \mu$m) with a peak power of about 1 MW. Using beam splitter BS and systems of mirrors M1−M3 together with doubled frequency crystal KTP the fundamental laser beam was split into two channels possessing beams with single and doubled frequencies. The latter, with the wavelength at 530 nm, was used as a pumping (photoinducing) beam. The second one at $\lambda = 1.06\ \mu$m passing through the delaying line (DL) was served as a probing one. The DL had retarded the probing polarized beam at 1.06 μm with respect to the pumping at 0.53 μm. The delaying time was changed from 5 ps to 50 ps. Shutter Sh has served for the closing of the pumping channel during photoinduced treatment and to control the scattering background from the fundamental laser beam. The pumping and probing polarized beams have been overlapped on the surface of the sample, S, and the grating spectrophotometer connected with the electronic boxcar has evaluated the output signal $I_{2\omega}$.

The laser light was polarized using a rotating Fresnel polarizer, P, and the output light intensity was detected using fast-response photomultipliers, PM. The measurements were carried out in the single-pulse regime with a pulse frequency repetition rate of 12 Hz and pump−probe pulse retardation equal to about 5−50 ps. Such short-time kinetics avoids specimen overheating. The pumping laser beam was scanned through the sample surface to obtain a larger number of measured points and to average statistically the sample's space nonhomogeneity. The pumping laser light and frequency-doubled light were spectrally separated using a grating monochromator (SPM-3M). During evaluation of the time-delayed nonlinear optical response, we measured the light intensities at ω and 2ω laser fundamental frequencies using the electronic boxcar in the time-synchronized pump−probe conditions. The second-order optical susceptibilities χ_{ijk} were evaluated numerically from the expression

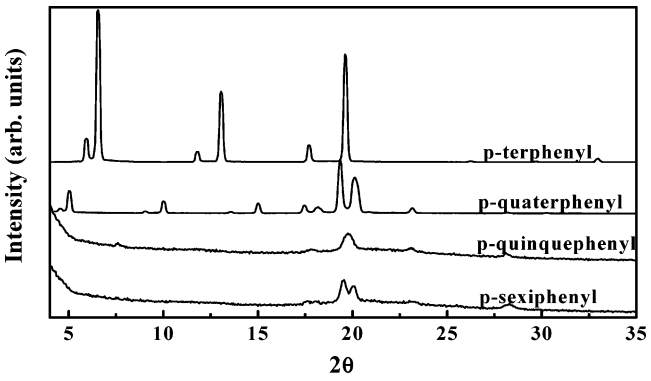

Figure 2. X-ray diffractograms of all of the considered samples.

$$I(2\omega,t) = \frac{2\mu_0^{3/2}n_0^{3/2}\alpha^2\chi_{ijk}^2 I(\omega,t-\tau)^2 d^2}{\pi R_0^2 n(2\omega)\,n(\omega)^2} \times \left[\frac{\sin(d\Delta k(t)/2)}{d\Delta k(t)/2}\right]^2 \quad (3)$$

where $n(\omega)$ and $n(2\omega)$ are the refractive indices for the pumping and second harmonic generation (SHG) doubled frequencies, respectively, obtained during the photopumping; χ_{ijk} are components of the second-order optical susceptibilities determined for different polarization angles of the incident light; μ_0 and ϵ_0 are the magnetic and dielectric static susceptibilities in vacuum; $\Delta k = k(2\omega) - 2k(\omega)$ is the phase-matching wave vector factor caused prevailingly by photoinduced birefringence. In our case the latter one was varied within the range $10^{-3}-10^{-2}$ to be estimated by the Senarmont method. The light intensities of the time-dependent pumping $I(\omega,t)$ and frequency-doubled signals $I(2\omega,t-\tau)$ were measured at different times (t) of pulse duration and for different delaying times (τ). From these values of t and τ we calculated the time-delayed second-order nonlinear optical susceptibilities, χ_{ijk}. Using a grating monochromator (spectral resolution about 7 nm/mm) connected to the boxcar, we determined the time-delayed χ_{ijk}. Moreover, we varied the angle of incidence to obtain additional equations determining the second-order optical susceptibilities. UV-absorption spectra were measured within the spectral range 200−700 nm. A multichannel analyzer was used to perform control of the signals, similar to that described in ref 21.

Results and Discussion

At the beginning, an optimization of geometry for all of the considered molecules was done. The completely optimized conformations of the quater-, quinque-, and sexiphenyl molecules present a significant deviation from planarity, which is in agreement with previous work.[22] Their aromatic rings are twisted, creating a rodlike molecule. The terphenyl structure is principally different compared to the samples with the larger number of aromatic rings because of its planar structure and absence of twisting.

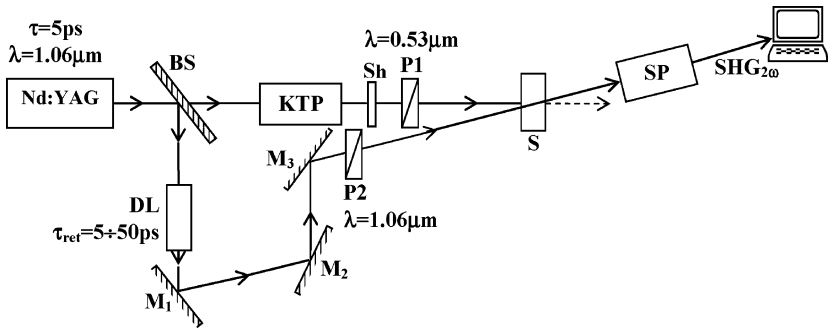

Figure 3. Setup for photoinduced SHG measurements. BS: beam splitter; M_1, M_2, M_3: mirrors; P1, P2: polarizer; DL: delayer of line; S: sample; Sh: shutter; SP: spectrograph.

TABLE 1: Principal Electronic Parameters of Considered Molecules: The Static Dipole Moment, μ, the HOMO−LUMO Splitting Gap, $\Delta E_{\text{HOMO-LUMO}}$, and the First Dipole-Allowed Electronic Excitation Energy[a]

molecule	μ (D)	$\Delta E_{\text{HOMO-LUMO}}$	λ_{0e} (eV)	λ_{exp} (nm)[a]
N-sexiphenyl	0.032	3.20	3.40 (λ_{0e} = 364.97 nm)	420
N-quinquephenyl	0.023	3.30	3.55 (λ_{0e} = 349.41 nm)	410
N-quaterphenyl	0.011	3.43	3.76 (λ_{0e} = 329.44 nm)	360
N-terphenyl	0.004	3.66	4.12 (λ_{0e} = 301.37 nm)	370
N-bephenyl	0.005	4.11	4.68 (λ_{0e} = 264.82 nm)	

[a] The experimentally obtained optical gaps are presented in the last column for comparison.

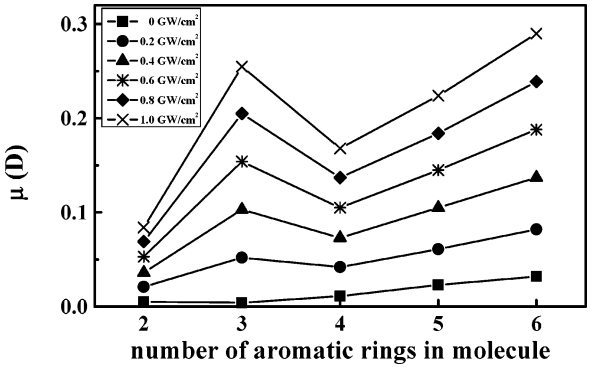

Figure 4. Changes of the static ground-state dipole momentums under the applied photoinduced power density.

The theoretical quantum chemical calculations were performed using the GRAC potential. This smooth potential is more preferable for calculation of optical response[13] for organic materials possessing π-conjugated bonds. The LDA calculations have yielded similar results. The principal electronic parameters computed for all of the considered molecules are presented in Table 1. The values of the ground-state dipole moments increase with increasing number of aromatic rings. Simultaneously, differences in energy between the HOMO and LUMO states decreases. The same behavior exhibits the first dipole-allowed electronic excitation energy. The values of all of the mentioned parameters are saturated with an increasing number of aromatic rings in the chain of the molecule. The presented results are in good agreement with the experimentally obtained data for *p*-sexiphenyl presented in ref 23.

In Figure 4, changes of the dipole moments for the investigated molecules at different power densities of photoinduced beam are shown. One can clearly see that without any external photoinducing treatment the dipole moments increase simultaneously with increasing number of aromatic rings for all of the considered phenyls, as shown in Table 1. It reflects a well-known fact that dipole moments of organic molecules increase simultaneously with elongation. It is necessary to emphasize

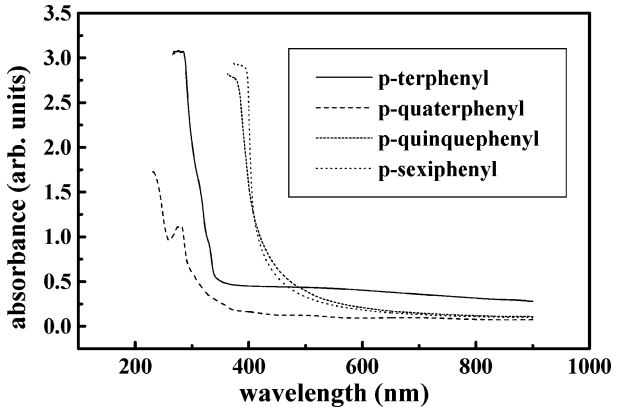

Figure 5. Experimental UV-absorption spectra for the investigated materials.

that when the photoinducing laser beam is used the value dipole moment for terphenyl increases more quickly than that for the remaining molecules. This fact is caused by bending of the aromatic rings for the compounds possessing higher numbers of aromatic films. To complete the presented considerations, we measured the UV-absorption spectra (see Figure 5). Optical gaps for all of the investigated samples evaluated from UV-absorption spectra are given in Table 1. The theoretically investigated as well as experimentally obtained data show a good correlation. One can conclude that the role of the particular intramolecular interaction is dominant for the linear optical properties of phenyls. The optical gap decreases with increasing number of aromatic rings. Only the terphenyl molecule demonstrates an exception, which may reflect its planar structure.

The hyperpolarizabilities $\beta_{\text{vec}}(-2\omega;\omega,\omega)$ calculated for all of the considered molecules versus photoinducing power densities are presented in Figure 6. These values were evaluated using the following formula

$$\beta_{\text{vec}}(-2\omega;\omega,\omega) = \sqrt{\beta_x^2(-2\omega;\omega,\omega) + \beta_y^2(-2\omega;\omega,\omega) + \beta_z^2(-2\omega;\omega,\omega)} \quad (4)$$

where $\beta_i(-2\omega;\omega,\omega) =$

$$\frac{1}{5}\sum_k (\beta_{ikk}(-2\omega;\omega,\omega) + 2\beta_{kki}(-2\omega;\omega,\omega)) \quad i = x, y, z \quad (5)$$

The obtained results show that with increasing pumping power density first-order nonlinear optical hyperpolarizability for sexiphenyl decreases contrary to the other phenyl molecule. Such behavior may be a consequence of "in vacuum" calculations, particularly, the internal molecular stereochemistry gives the dominant contribution to microscopic second-order NLO properties. Moreover, one can guess that it is crucial for a longer

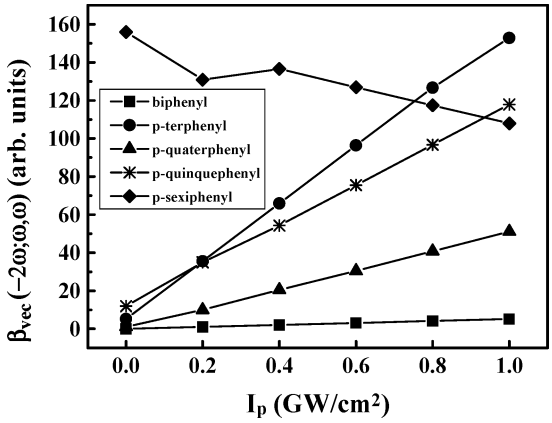

Figure 6. Calculated hyperpolarizability $\beta_{vec}(-2\omega;\omega,\omega)$ value for all of the considered molecules versus photoinduced power density.

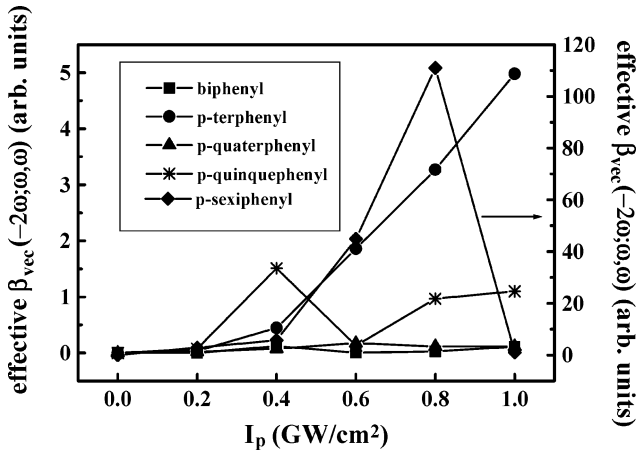

Figure 7. Calculated first-order hyperpolarizability $\beta_{vec}(-2\omega;\omega,\omega)$ value for all of the considered molecules versus photoinduced power density, taking into account the reorientation of the molecule.

molecule. In this case, the twisting of the aromatic rings may cause a compensation of the particular dipole moments.

The existing quantum chemical calculations[24,25] consider the *N*-phenyl investigated material to be an isolated molecule, which means that the amorphous-like environment does not disturb the partial ordering of the molecules.

Let us go from the separated molecule to the aligned molecules incorporated into the amorphous-like background under the influence of an external electric field. In this case, the increase of the effective first-order nonlinear optical hyperpolarizability seems to be sufficiently different compared to the properties of the single molecule (see Figure 7). The value depicted on the *y* axis, (here called the effective first-order optical hyperpolarizability), was evalauted by multiplying the molecular first-order nonlinear optical hyperpolarizability, presented in Figure 6, by the order parameters mentioned in eqs 1 and 2. The order parameters depend on the scalar product of the molecular excited-state dipole moments, $\vec{\mu}$, and the external electric field, $\vec{E}$. For the investigated systems, the order parameters were theoretically predicted assuming a thermodynamic equilibrium Boltzman distribution of molecules. In ref 26, an agreement was demonstrated between the MD simulated value of the order parameters and the odd-order Langevin functions $L_1(p)$ and $L_2(p)$ for the rodlike molecules. Therefore, one can conclude that the odd-order Langevin functions can reproduce the simulated order parameters sufficiently well. A particular difference between the first-order nonlinear optical hyperpolarizability calculated for the isolated molecule and the

TABLE 2: Structural Weighting Parameters Computed for Considered Systems Using Equation 5

molecule	crystal structure x (%)	amorphous structure $1 - x$ (%)
N-sexiphenyl	30 ± 10	70 ± 10
N-quinquephenyl	60 ± 8	40 ± 8
N-quaterphenyl	70 ± 6	30 ± 6
N-terphenyl	65 ± 6	35 ± 6

effective first-order nonlinear optical hyperpolarizability has appeared only for the case of the sexiphenyl molecule. The first-order nonlinear optical hyperpolarizability calculated for sexiphenyl in vacuum decreases simultaneously with increasing pumping power density, but the effective first-order nonlinear optical hyperpolarizability increases for the pumping power density up to 0.8 GW/cm^2. The power density equal to 0.8 GW/cm^2 strongly aligns the sexiphenyl molecules because of the higher value of its dipole moment in the excited state compared to other compounds.

From the X-ray diffractograms presented in Figure 1, one can see that the *p*-terphenyl and *p*-quaterphenyl samples are more long-range ordered than *p*-quinquephenyl and *p*-sexiphenyl. To compare the changes of experimentally obtained and computed effective first-order nonlinear susceptibilities, one should take into account the crystal and amorphous NLO response contribution. We performed a calculation of the first-order nonlinear optical susceptibility versus the power density of the pumping laser beam for the considered systems by eqs 1and 2 with order parameters for the disordered structure and for the crystal structure, assuming that all of the molecules are perfectly aligned along the *z* axis. Calculating the effective first-order nonlinear optical susceptibility for the composition of the amorphous and long-range ordered (crystal) system, we have introduced a structural weighting factor

$$\chi_{vec} = x \cdot \chi_{vec}^{crystal} + (1 - x) \cdot \chi_{vec}^{amorphous} \quad (6)$$

where x and $(1 - x)$ are the structural weighting factors defining the partial contribution of the crystalline and amorphous-like structure, respectively.

Figure 8 shows the experimental and theoretical data for the effective first-order nonlinear optical susceptibilities computed by eqs 1, 2, and 6. For all of the considered films, the structural weighting factors have been found by fitting the theoretically obtained curves to the experimentally measured data, and the obtained data are presented in Table 2. The local field factors presented in eqs 1 and 2 were evaluated within a framework of the Onsager approach.[27]

From Figure 8 one can see that all of the experimental data demonstrate an occurrence of the SHG maximum versus pump-power density. The same behavior was obtained for all of the simulated molecules excluding *p*-terphenyl, for which the computed optical susceptibility continuously increases. This is because the $\beta_{vec}(-2\omega;\omega,\omega)$ value calculated for *p*-terphenyl increases drastically with increasing power density of the photoinducing beam. It is also necessary to emphasize that the *p*-terphenyl is a very photoactive (photosensitive) molecule, which is probably a cause of the specific values of the transition dipole moments, particularly, it has a very intensive absorption band.[28] It is necessary again to emphasize that *p*-terphenyl is a perfectly planar molecule compared to other investigated phenyls (with higher *N*). The anisotropy and photoinducing polarized optical wave enhance its dipole moment and hyperpolarizability.

In ref 6 it was shown that for the investigated molecules a dominant mechanism determining the charge transport properties

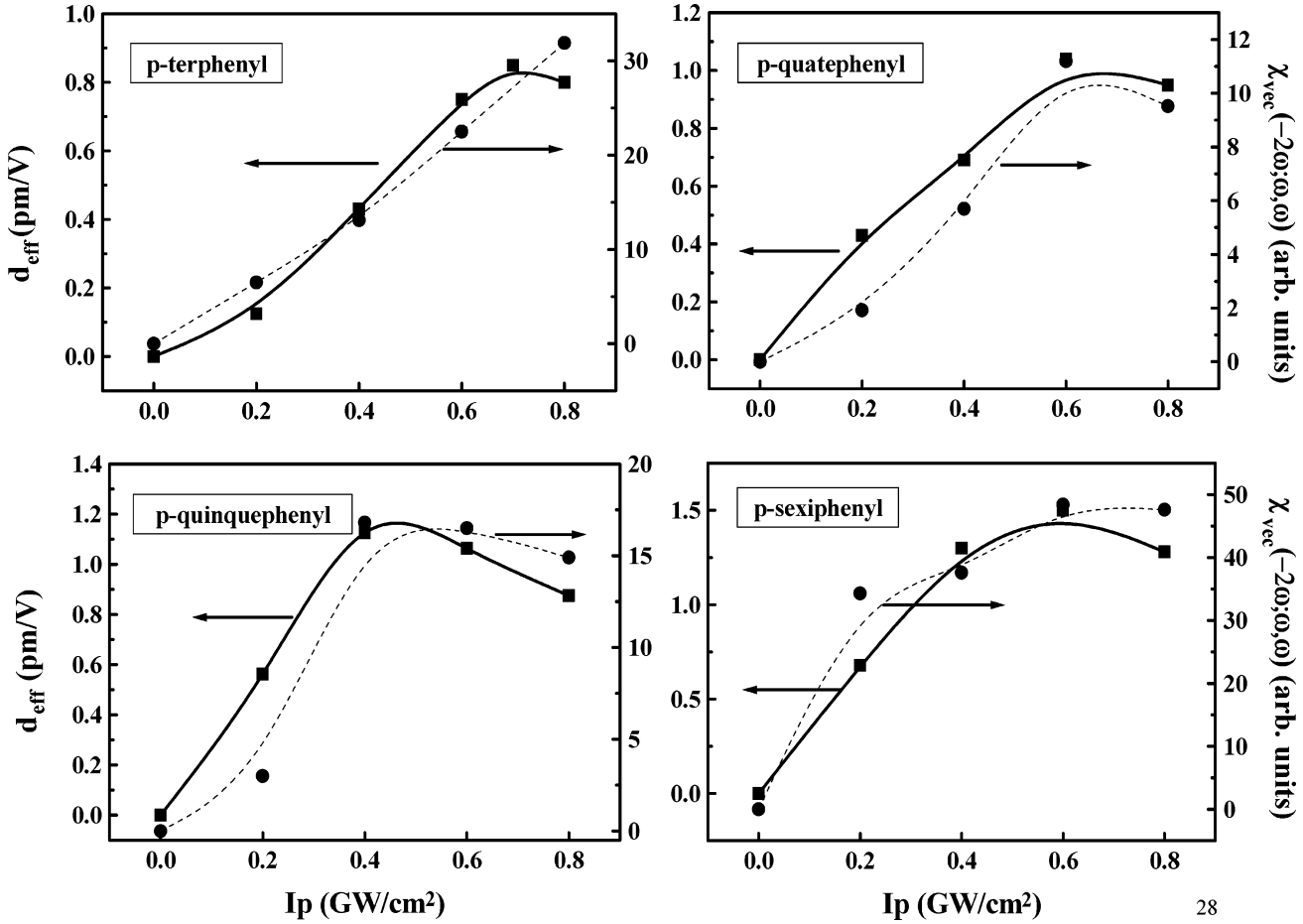

Figure 8. Dependence of the photoinduced second-order optical susceptibility versus the photoinduced power density for sexiphenyl. Experimental data: squares (solid line: fitted experimental data); and theoretical results: circles (dashed line: fitted theoretically obtained data).

is caused by a nanointerface region. From general consideration, one can think that the same situation should be with optical and nonlinear optical properties. However, considering the theoretically and experimentally obtained results one can see that interpreting the nonlinear optical properties is necessary to take into account for substantial contribution of amorphous-like and crystalline phase for all of the considered samples. One can say that for the nonlinear optical properties the so-called bulklike contribution plays a prevailing role. It may be a consequence of different occupation photokinetics of the particular localized levels for these two different phenomena. During the transport phenomena, the great role belongs to the activation jumping between the particular electronic levels of the interface region.

As a consequence, manifestation of the considered structural fragments in the nonlinear optical properties may be different compared to the transport properties (particularly DC conductivity).

Conclusions

Using a conception of the coexistence of amorphous and crystalline-like phases in the *N*-phenyls, we have explained an origin of their photoinduced SHG phenomena. It was established that the role of the interface region between microcrystallites and amorphous background is not as crucial for the first-order nonlinear optical hyperpolarizabilities as for the transport properties (particularly DC conductivity). The photoinduced SHG behavior of the *N*-phenyls can be fairly well reproduced like superposition of the crystalline and amorphous-like phase of the media using as a fitting scaling factor obtained from the X-ray difractometry. The optical susceptibility of the considered structures can be calculated in a simple local field factor model. Differences between the experimentally measured and theoretically computed results are observed only for the *p*-terphenyl films, which probably reflects the specific photoactivity features of the films and their plane structure. Its photoactivity enhances the internal charge transfer of the molecule, which affects the regularity of the charge density distribution. A more hyperfine model should be developed to map the nonlinear optical properties for the molecule with nonhomogeneous charge density distribution. Particularly, it is necessary to include the dipole−dipole interaction, inducing charge interaction and a discrete local field model.

References and Notes

(1) *Polymers for Lightwave and Integrated Optics: Technology and Applications*; Hornak, L. A., Ed.; Marcel Dekker: New York, 1992.

(2) Chemla, D. S.; Zyss, J. *Nonlinear Optics*,; Academic Press: New York, 1974.

(3) Tkaczyk, S. *Synth. Met.* **2000**, *109*, 249.

(4) Tkaczyk, S.; Kityk, I. V. *Appl. Surf. Sci.* **2005**, *241*, 287.

(5) Tkaczyk, S.; Kityk I. V. Schiffer, R. *Phys. D* **2002**, *35*, 563

(6) Tkaczyk, S.; Kityk, I. V.; Viennois, R. *J. Chem. Phys.* **2004**, *121*, 1.

(7) Murzina, T. V.; Misuryaev, T. V.; Nikulin, A. A.; Aktsipetrov, O. A.; Güdde, J. *J. Magn. Magn. Mater.* **2003**, *258*−*259*, 99.

(8) Williams, D. J. Nonlinear Optical Properties of Guest−Host Polymer Structures. In *Nonlinear Optical Properties of Organic Molecules and Crystals*; Chemla, D. S., Zyss, J., Eds.; Academic Press: New York, 1987.

(9) (a) Velde, G.; Baerends, E. J. *J. Comput. Phys.* **1992**, *99*, 84. (b) van Gisbergen, S. J. A.; Snijders, J. G.; Baerends, E. J. *J. Comput. Phys.*

1999, *118*, 119. (c) Baerends, E. J.; Berces, A.; Bo, C.; Boerribter, P. M.; Cavallo, L.; Deng, L.; Dickson, R. M.; Ellis, D. E.; Fan, L.; Fisher, T. H.; Fonseca Guerra, C.; van Gisbergen, S. J. A.; Groeneveld, J. A.; Gritsenko, O. V.; Harris, F. E.; van den Hoek, P.; Jacobsen, H.; van Kessel, G.; Kootstra, F.; van Lenthe, Om, V. P.; Relasesinga, P. H. T.; Philipsen, D.; Post, C. C.; Pye, W.; Ravenek, P.; Ros, P. R. T.; Schipper, G.; Schreckenbach, Snijders, J. G.; Sola, M.; Swerhone, D.; Velde, G.; Vernooijs, P.; Versluis, L.; Visser, O.; van Wezenbeek, E.; Wiesenekker, G.; Wolff, S. K.; Woo, T. K.; Ziegler, T. *ADF Program System*, Release 2004.01

(10) (a) Runie, E.; Gross, E. K. U. *Phys. Rev. Lett.* **1984**, *52*, 997. (b) Gross, E. K. U.; Kohn, W. *Adv. Quantum Chem.* **1990**, *21*, 255. (c) van Leeuwen, R. *Int. J. Mod. Phys. B* **2001**, *15*, 1969. (d) van Gisbergen, S. J. A. *Molecular Response Property Calculations using Time-Dependent Density Functional Theory, in Chemistry*; Vrije Universiteit: Amsterdam, 1998; p 190.

(11) Gross, E. K. U.; Dobson, J. F. In *Density Functional Theory*; Nalewajski, R. F., Ed.; Springer: Heidelberg, 1996.

(12) van Gisbergen, S. J. A.; Snijders, J. G.; Baerends, E. J. *Comput. Phys*. **1999**, *118*, 119.

(13) (a) van Gisbergen, S. J. A.; Snijders, J. G.; Baerends, E. J. *J. Chem. Phys*. **1998**, *109*, 10644. (b) Cohen, A. J.; Handy, N. C.; Tozen, D. J. *J. Chem. Phys. Lett.* **1999**, *303*, 391. (c) Riccardi, G.; Rosa, A.; van Gisbergen, S. J. A.; Baerends, E. J. *J. Phys. Chem. A* **2000**, *104*, 635. (d) te Velde, G.; Bickelhaupt, F. M.; Baerends, E. J.; Fonseca Guerra, C.; van Gisbergen, S. J. A.; Snijders, J. G.; Ziegler, T. *J. Comput. Chem*. **2001**, *22*, 931.

(14) van Faassen, M.; Boeij, P. L.; van Leeuwen, R.; Berger, J. A.; Snijders, J. G. *Phys. Rev. Lett.* **2002**, *88*, 186401.

(15) Gruning, M.; Gritsenko, O.; van Gisbergen, S. J. A.; Baerends, E. J. *J. Chem. Phys*. **2001**, *114*, 652.

(16) Vosko, S. H.; Wilk, L.; Nusair, M. *Can. J. Phys*. **1980**, *58*, 1200.

(17) (a) Dunning, J. *J. Chem. Phys.* **1971**, *55*, 716. (b) Dyall, K. G. *Theor. Chem. Acc*. **2002**, *108*, 335; erratum *Theor. Chem. Acc*. **2003**, *109*, 284.

(18) Perdew, J. P. *Phys. Rev. B* **1986**, *33*, 8822.

(19) Becke, A. D. *Phys. Rev. A* **1988**, *38*, 3098.

(20) Yang, P. K.; Huang, J. Y.; Jou, J. H. *Proc. Natl. Sci. Counc*. **2000**, *24*, 310.

(21) Kityk, I. V. *J. Mod. Opt.* **2004**, *51*, 1179.

(22) Brocorens, P.; Zojer, E.; Cornil, J.; Shuai, Z.; Leising, G.; Muller, K.; Bredas, J. L. *Synth. Met.* **1999**, *100*, 141; and works cited there.

(23) Kajii, H.; Tsukagawa, T,; Okuno, H.; Taneda, T.; Yoshino, K.; Ohmori, Y. *Thin Solid Films* **2001**, *393*, 388.

(24) Koch, N.; Parente, L. M. V.; Lazzaroi, R.; Johnson, R. L.; Leising, G.; Pireaux, J. J.; Bredas, J. L. *Synth. Met.* **1999**, *101*, 438.

(25) Furuya, K.; Torii, H.; Furukawa, Y.; Tasumi, M. *J. Mol. Struct.: THEOCHEM* **1998**, *424*, 225.

(26) Makowska-Janusik, M.; Reis, H.; Papadopoulos, M. G.; Economou, I. G.; Zacharopoulos, N. *J. Phys. Chem. B* **2004**, *108*, 588.

(27) (a) Onsager, L. *J. Am. Chem. Soc.* **1936**, *1486*, 58. (b) Andersena, J. U.; Bonderup, E. *Eur. Phys. J. D* **2000**, *11*, 435.

(28) Adachi, C.; Tsutsui, T.; Saito, S. *Appl. Phys. Lett.* **1990**, *56*, 799.